

## ARTICLE OPEN



# Multimomics analysis of serial PARP inhibitor treated metastatic TNBC inform on rational combination therapies

Marilyne Labrie<sup>1,2</sup>✉, Allen Li<sup>1</sup>, Allison Creason<sup>3</sup>, Courtney Betts<sup>2</sup>, Jamie Keck<sup>1,4</sup>, Brett Johnson<sup>1,4,5</sup>, Shamilene Sivagnanam<sup>1,3</sup>, Christopher Boniface<sup>6</sup>, Hongli Ma<sup>1,2</sup>, Aurora Blucher<sup>1,2</sup>, Young Hwan Chang<sup>3,4,5</sup>, Koei Chin<sup>4,5</sup>, Jacqueline Vuky<sup>1</sup>, Alexander R. Guimaraes<sup>1,7</sup>, Molly Downey<sup>8</sup>, Jeong Youn Lim<sup>1</sup>, Lina Gao<sup>1</sup>, Kiara Siex<sup>1</sup>, Swapnil Parmar<sup>1</sup>, Annette Kolodzie<sup>1,4</sup>, Paul T. Spellman<sup>1,4,6</sup>, Jeremy Goecks<sup>3</sup>, Lisa M. Coussens<sup>1,2</sup>, Christopher L. Corless<sup>1,8</sup>, Raymond Bergan<sup>1</sup>, Joe W. Gray<sup>1,4,5</sup>, Gordon B. Mills<sup>1,2,9</sup> and Zahi I. Mitri<sup>1</sup>✉

In a pilot study, we evaluated the feasibility of real-time deep analysis of serial tumor samples from triple negative breast cancer patients to identify mechanisms of resistance and treatment opportunities as they emerge under therapeutic stress engendered by poly-ADP-ribose polymerase (PARP) inhibitors (PARPi). In a BRCA-mutant basal breast cancer exceptional long-term survivor, a striking tumor destruction was accompanied by a marked infiltration of immune cells containing CD8 effector cells, consistent with pre-clinical evidence for association between STING mediated immune activation and benefit from PARPi and immunotherapy. Tumor cells in the exceptional responder underwent extensive protein network rewiring in response to PARP inhibition. In contrast, there were minimal changes in the ecosystem of a luminal androgen receptor rapid progressor, likely due to indifference to the effects of PARP inhibition. Together, identification of PARPi-induced emergent changes could be used to select patient specific combination therapies, based on tumor and immune state changes.

*npj Precision Oncology* (2021)5:92; <https://doi.org/10.1038/s41698-021-00232-w>

## INTRODUCTION

Triple negative breast cancer (TNBC) is characterized by lack of expression of estrogen (ER) and progesterone (PR) receptors and human epidermal growth factor receptor 2 (HER2). Despite advances in our understanding of TNBC biology, metastatic TNBC (mTNBC) remains an incurable disease, with limited therapeutic options and high mortality. A key to developing therapies that induce durable responses is the recognition that TNBC represents a molecularly heterogeneous disease with several clinically relevant subtypes. Indeed, some of the “failures” of clinical trials in mTNBC may be due to the heterogeneous nature of the disease, such that therapies are not tested against the appropriate subsets. A precision oncology approach of targeting therapeutic liabilities as they arise in response to therapy in mTNBC may increase the efficiency of selection of patient specific combination therapy.

Recent clinical trials have aimed at capitalizing on molecular alterations in mTNBC to implement effective novel therapies. For patients with germline *BRCA* mutations, the PARP inhibitors olaparib and talazoparib are now FDA-approved, based on improved efficacy and safety of PARPi therapies compared to cytotoxic chemotherapies<sup>1–3</sup>. Additionally, immune checkpoint blockade (ICB) therapy in combination with chemotherapy was approved for frontline treatment of mTNBC expressing PD-L1 based on improved progression-free and overall survival<sup>4,5</sup>. However, despite these promising advances, virtually all patients develop progressive disease on PARPi- or ICB-based therapies, indicating a critical need to implement patient specific

combinations that can interdict or overcome resistance as it emerges in mTNBC.

The combination of PARPi and ICB is effective in breast cancer models wild-type for *BRCA1/2* and competent for DNA damage repair. These models have shown induction of a stimulator of interferon genes (STING) response that induces interferon production and immune activation<sup>6–9</sup>. The MEDIOLA and TOPACIO trials both demonstrated that PARPi and ICB combinations are well tolerated and have clinical activity in a subset of both *BRCA*-mutant as well as *BRCA*-wild type solid tumors, albeit with much more limited activity in *BRCA*-wild type tumors<sup>10–12</sup>. Unfortunately, serial biopsies were only available on a limited number of patients in these studies, precluding identification of predictive biomarkers and resistance mechanisms that enabled tumors to eventually escape control. This is especially important because although a number of predictors of PARPi mono and combination therapy have been proposed, these do not accurately predict which metastatic breast cancer patients are likely to obtain benefit from PARPi mono and combination therapies. Indeed, there remains patients without the current biomarkers who benefit and patients with the best predictive biomarkers who do not benefit. Thus there is a need to go beyond our current analysis and identify better approaches to more fully identify patients likely to benefit.

Tumors and the tumor ecosystem rapidly adapt to therapeutic stress on treatment with therapeutic agents, including PARPi. These adaptive responses indicate both mechanisms of resistance and therapeutic opportunities. We and others have demonstrated that combination therapy designed to capitalize on adaptive

<sup>1</sup>Knight Cancer Institute, Oregon Health and Science University, Portland, OR, USA. <sup>2</sup>Department of Cell, Developmental & Cancer Biology, Oregon Health and Science University, Portland, OR, USA. <sup>3</sup>Computational Biology Program, Oregon Health and Science University, Portland, OR, USA. <sup>4</sup>Center for Spatial Systems Biomedicine (OCSSB), Oregon Health and Science University, Portland, OR, USA. <sup>5</sup>Department of Biomedical Engineering, Oregon Health and Science University, Portland, OR, USA. <sup>6</sup>Department of Molecular and Medical Genetics, Oregon Health and Science University, Portland, OR, USA. <sup>7</sup>Department of Diagnostic Radiology, Oregon Health and Science University, Portland, OR, USA. <sup>8</sup>Department of Pathology, Oregon Health and Science University, Portland, OR, USA. <sup>9</sup>Department of Systems Biology, The University of Texas MD Anderson Cancer Center, Houston, TX, USA. ✉email: labriem@ohsu.edu; mitri@ohsu.edu

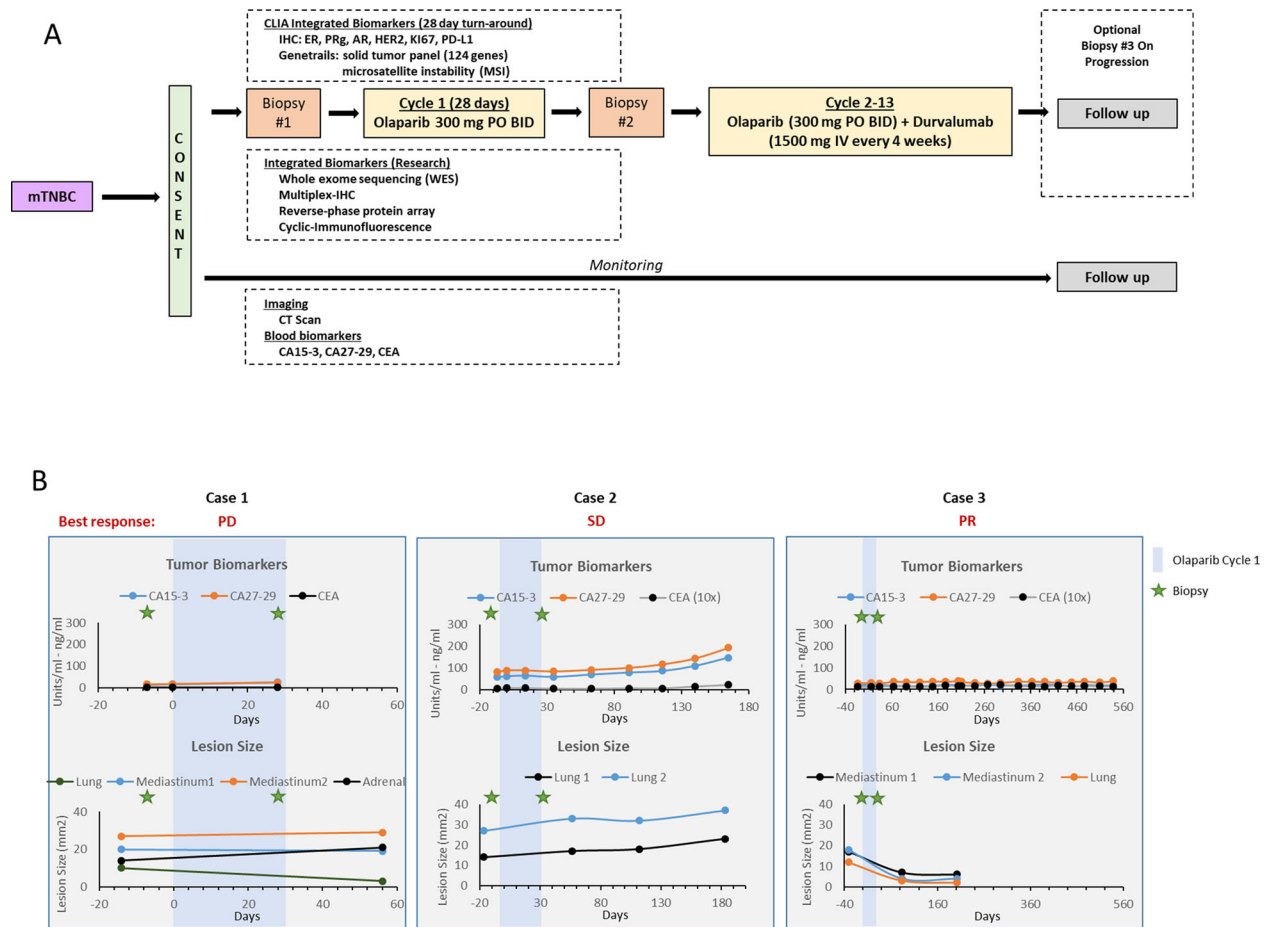


**Fig. 1 Schematic of study design and patient's response to olaparib and durvalumab combination.** **a** After consent, mTNBC patients were subjected to a pre-treatment biopsy (#1) followed by one cycle of olaparib (28 days) and an on-treatment biopsy (#2). Patients were then treated with a combination of olaparib and durvalumab for up to 12 additional cycles. **b** (Upper panel) Blood biomarkers, (lower) lesion size. Green stars represent the time of pre and on-treatment biopsies collection and the blue bar represent the first cycle of olaparib monotherapy, which started on day 0.

responses induced by therapy can generate tumor control in preclinical model systems<sup>13–23</sup>. We have translated many of these observations to clinical trials, with marked patient benefit (NCT03162627, NCT02208375, NCT02659241, NCT03586661, NCT02316834, NCT03544125, NCT03801369, and NCT03637491). While analysis of baseline and on-therapy biopsies provides significant information, the information content on changes induced by therapy appears to provide additional information that could potentially be used for selection of combination therapies following validation in larger studies<sup>18</sup>.

This pilot clinical trial (NCT03544125) evaluated the safety and efficacy of the combination of olaparib and durvalumab for treatment of mTNBC patients and feasibility of longitudinal analysis of serial tumor samples in real-time to identify adaptive mechanisms of resistance as they emerge under PARPi therapeutic stress (Fig. 1). This study incorporated comprehensive multi-omics analysis of serial liquid and tumor biopsies under the precision oncology platform: Serial Measurements of Molecular and Architectural Responses to Therapy (SMMART) at the Oregon Health & Science University Knight Cancer Institute (OHSU KCI)<sup>24</sup>. The SMMART analytic platform and robust computational biology pipeline enables study of adaptive mechanisms of resistance as they emerge and offers a new design of biomarker-driven clinical trials aimed at identifying markers of benefit as well as selecting combinations of drugs in real-time to benefit the patient under therapy.

## RESULTS

### Patient characteristics

From 5/14/2018 to 7/24/2018, three participants with mTNBC were enrolled in the pilot study and successfully underwent pre-treatment biopsy, one cycle of olaparib monotherapy, and a repeat on-treatment biopsy before starting the olaparib and durvalumab combination. Table 1 depicts the baseline characteristics of each patient. Median age of participants was 51.3 years old (range 39–66). All participants had more than three sites of metastatic disease, including visceral disease. All participants had received either prior neoadjuvant or adjuvant chemotherapy; none had prior systemic therapy for metastatic disease. Only one patient (case 3) had a BRCA1 germline deletion in exon 13–15, although this deletion is of unknown significance.

### Feasibility

All three participants completed the scheduled pre- and on-treatment biopsies of metastatic tumor. With the exception of two assays, all predetermined CLIA analytics on the pre-treatment biopsy specimens were completed within the previously defined 4-week window prior to the on-treatment biopsy. As shown in Supplementary Table 4, the median time of completion was 13 days, meeting the primary endpoint of feasibility of completing CLIA analytics.

**Table 1.** Patient's characteristics.

	Case 1	Case 2	Case 3
<b>Demographics</b>			
Age	49	39	66
Race	white	white	white
ECOG	1	0	0
<b>Disease characteristics</b>			
Receptor status at diagnosis	ER < 1%, PR 0%, Her2 0%, AR 100%	ER 0%, PR 0%, Her2 1+, AR 0%	ER 0%, PR 0%, Her2 1+, AR 0%
Histology	IDC	IDC	IDC
Disease stage	metastatic	metastatic	metastatic
Metastatic sites	lung, mediastinal LN, upper gastrohepatic LNs, adrenal glands, bone	lungs, hilar LNs, chest wall	CNS, lung, hilar and mediasinal LN, subcutaneous
Site of metastasis	> 3	> 3	> 3
<b>Prior therapy</b>			
Neoadjuvant or adjuvant	AC x 4c	AC x 2c, TC x 2c	AC-T
Adjuvant radiation	yes	yes	no
Disease-free interval	1 mo	5 mo	46 mo
Metastatic systemic treatment	none	none	none
Surgery	bilateral mastectomies	lumpectomy	bilateral mastectomies
<b>Olaparib/durvalumab</b>			
Best response	PD	SD	PR
Best response duration	PD	7 mo	15.1
Overall response	PD	PD	PD
Survival (months)	1.77	12.53	Not reached

ECOG Eastern Cooperative Oncology Group, IDC invasive ductal carcinoma, ER estrogen receptor, PR progesterone receptor, HER2 human epidermal growth factor receptor 2, AR androgen receptor, LN lymph node, CNS central nervous system, AC adriamycin/cyclophosphamide, T paclitaxel, TC taxotere/cyclophosphamide, PD progressive disease, SD stable disease, PR partial response.

## Safety

The safety of olaparib and durvalumab drug combination has been explored in previous studies<sup>11,12</sup>. In this pilot study, there were no adverse events (AE) related to pre- and on-treatment biopsies in all three patients. Only one grade 3–4 event was noted in the patients, which consisted of a hip fracture in a patient with known bone involvement and was considered unrelated to treatment (Table 2). All other events were grade 1–2, with the most common AEs being fatigue ( $n = 2/3$ ), nausea ( $n = 2/3$ ), constipation ( $n = 2/3$ ), and muscular skeletal pain ( $n = 2/3$ ). There were no AEs that led to treatment discontinuation. No immune-related AEs were observed.

## Case 1

49 year-old Caucasian woman with a history of stage I (T1cN0M0) invasive ductal carcinoma (IDC), ER/PR positive, HER2 non-amplified, treated with lumpectomy and SLN evaluation, followed by adjuvant taxotere/cyclophosphamide (TC) chemotherapy for 4 cycles. Upon loco-regional recurrence, a new biopsy showed TNBC disease, and she subsequently underwent bilateral mastectomies and lymph node evaluation, followed by adriamycin/cyclophosphamide (AC) for 4 cycles, and radiation therapy. She presented shortly after radiation therapy with biopsy-proven high grade mTNBC involving lungs, mediastinal and upper gastrohepatic lymph nodes, right adrenal gland, and bones (Table 1). At 14 days after metastatic disease diagnosis, the patient received treatment on study, with a best response of progressive disease (PD). The patient developed rapid progression and passed away after 2 months on therapy. During the course of treatment, the patient did not have elevated serum tumor markers (CA15-5, CA27-29, or CEA). Two lesions remained stable, one decreased and one

**Table 2.** Adverse events.

Grade	AEs	% ( $n = 3$ )
Grade 3–4	Hip fracture <sup>a</sup>	33% (1)
Grade 1–2	Fatigue	66% (2)
	Neutropenia	33% (1)
	Anemia	33% (1)
	Thrombocytopenia	33% (1)
	Hypocalcemia	33% (1)
	Hypomagnesemia	33% (1)
	Nausea	66% (2)
	Emesis	33% (1)
	Sun sensitivity	33% (1)
	Rash	66% (2)
	Ecchymosis	33% (1)
	Diarrhea	33% (1)
	Constipation	66% (2)
	Muscular skeletal pain	66% (2)
Headache	33% (1)	
Chills	33% (1)	

<sup>a</sup>Not treatment related.

increased in size (Fig. 1b). Both pre- and on-olaparib biopsies were acquired from a mediastinal lymph node. H&E staining of both biopsies showed similar histopathological features, with over 90% tumor content and little immune cell infiltration (Fig. 2a). Pre and



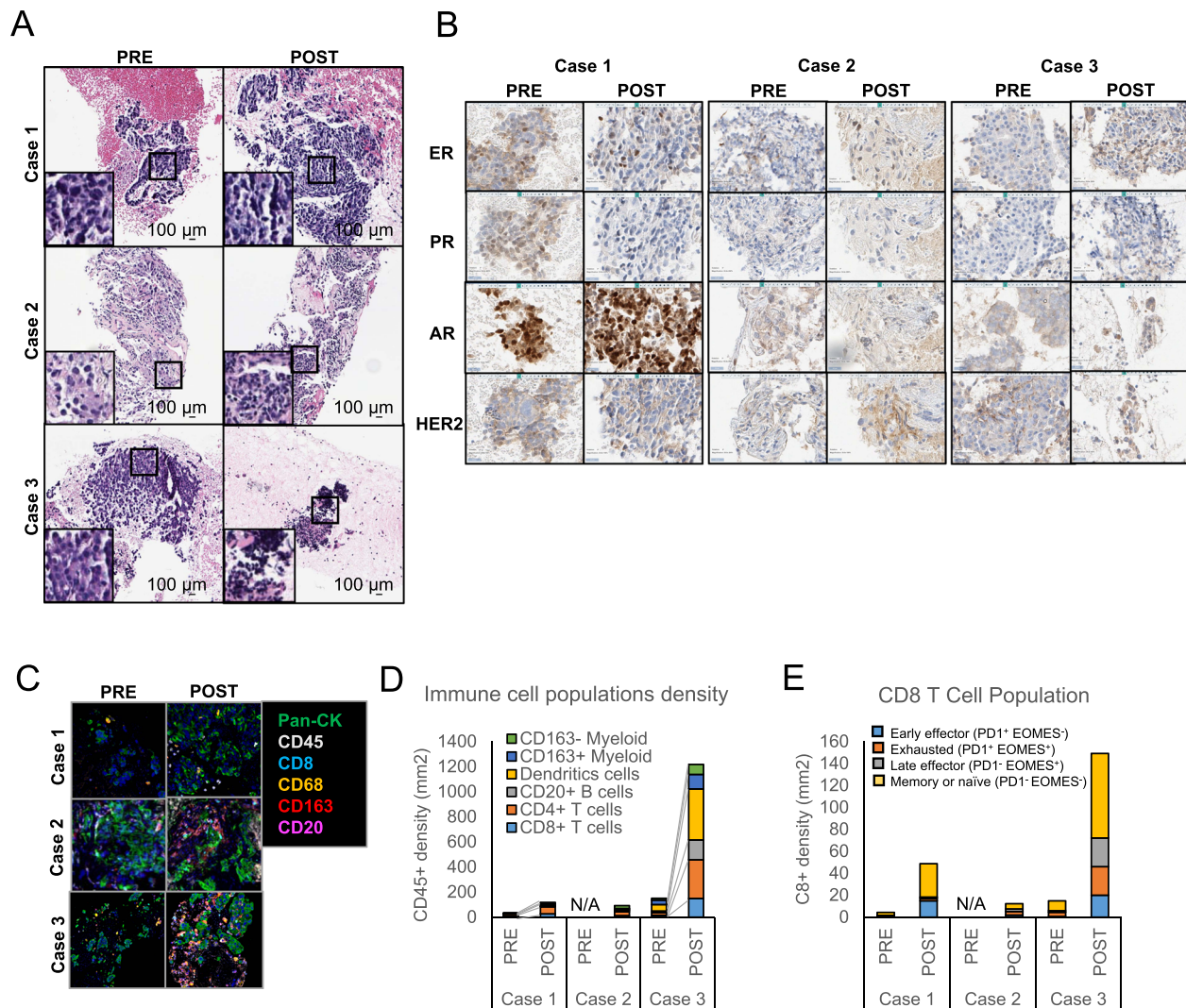


**Fig. 2 Tumors histopathological phenotype and immune composition.** **a** An H&E and **b** CLIA IHC staining of estrogen receptor (ER), progesterone receptor (PR), androgen receptor (AR) and human epidermal growth factor receptor 2 (HER2) was performed on both pre and on-treatment biopsies for each patient. mIFC was used to **c** reconstruct a region of each tumor showing epithelial cells (pan-CK) and various immune cells subtypes as indicated, **d** identification of immune cell population subset and density, and **e** determination of CD8<sup>+</sup> T cell population characteristics based on expression of PD-1 and EOMES expression.

on-treatment samples were negative for hormone receptors, except for strong nuclear expression of the androgen receptor (AR) (Fig. 2b). In addition, the on-treatment sample had 5% estrogen expressing cells. Ki67 decreased from 50% in the pre-treatment sample to 30% in the on-treatment sample. PD-L1 was positive low in both samples (1–10% and 10–20% respectively) (Table 3). GeneTrails<sup>®</sup> Comprehensive Tumor Panel and WES showed mutations in *TP53* and *FGFR4* variant of unknown significance (VUS) as well as amplification of *CCND1* and *FGF3* (Table 3). The full list of SNVs and CNVs from WES can be found in Supplementary Tables 5 and 6, respectively.

### Case 2

39 year-old Caucasian woman with a history of stage IIa (T2N0M0) triple negative IDC, treated with lumpectomy, sentinel node biopsy, AC × 2 cycles (stopped due to toxicity), and taxotere/cyclophosphamide (TC) × 2 cycles. She had a first loco-regional recurrence 4 months after initial therapy, treated with modified radical mastectomy followed by 2 cycles of TC and adjuvant radiation therapy. The patient presented with biopsy-proven high-grade mTNBC involving lungs, hilar lymph nodes, and chest wall

(Table 1). The patient was on study 125 days after metastatic disease diagnosis. The best response was stable disease (SD) for 7 months prior to progression, and survival of 12.5 months. During the course of treatment, the patient had gradual increases in CA15-5, CA27-29 and CEA that accelerated rapidly prior to death. Two lung lesions slightly increased in size during therapy (Fig. 1b). Both pre and on-olaparib biopsies were acquired from the lung. H&E stained sections showed similar histopathological features in the pre- and on-therapy samples, with over 90% tumor content and minor immune cell infiltration (Fig. 2a). Both biopsies were negative for hormone receptors (Fig. 2b). Ki67 increased from 50% in the pre-treatment sample to 80% on-treatment. PD-L1 was negative in the on-treatment biopsy (pre-treatment biopsy was insufficient for testing) (Table 3). GeneTrails<sup>®</sup> Comprehensive Tumor Panel and WES analysis revealed mutations in *TP53*, *RB1*, *ALK* VUS, and *MDC1* VUS (Table 3). The full list of SNVs and CNVs from WES can be found in Suppl. Table 5 and 6, respectively.

### Case 3

66 year-old Caucasian woman with a history of stage I multi-focal invasive IDC, with three lesions triple negative and one weakly ER

**Table 3.** Tumor's characteristics.

Biopsy	Case 1		Case 2		Case 3	
	Pre	Post	Pre	Post	Pre	Post
ER	Neg	5%	Neg	Neg	Neg	Neg
PR	Neg	Neg	Neg	Neg	Neg	Neg
HER2	Neg	Neg	Neg	Neg	Neg	Neg
AR	100%	100%	Neg	Neg	Neg	Neg
Ki67	50%	30%	50%	80%	60–80%	50%
PD-L1	1–10%	10–20%	n/a	Neg	Neg	n/a
CNA (Copies)	CCND1 (84), FGF3 (44)	CCND1 (51), FGF3 (45)	ND	ND	MYC (8.5), RB1 (0.96)	n/a
SNV (%VAF)	TP53 (63%), FGFR4 (64%)	TP53 (86%), FGFR4 (65%)	RB1, TP53, ALK, MDC1	RB1, TP53, ALK, MDC1	TP53 (70%)	n/a
MSI	Stable	Stable	Stable	Stable	Stable	n/a

ND none detected, n/a not available.

positive (11%), treated with bilateral nipple sparing mastectomy, adjuvant AC, and taxol chemotherapy. This was followed by anastrozole adjuvant therapy for the weakly ER positive tumor. She developed local regional recurrence in the chest wall after 2 years. Excisional biopsy showed ER negative, PR negative, HER2 normal invasive ductal cancer. She was treated with carbo/gemcitabine followed by radiation therapy. She did well for 5 years when she presented with a subcutaneous mass in the umbilicus. The biopsy again demonstrated TNBC. Imaging showed evidence of metastatic disease involving brain, lung, hilar and mediastinal lymph nodes. (Table 1). The patient was enrolled in the study 85 days after metastatic disease diagnosis and experienced a partial response (PR; near complete). She had progression of disease in hilar lymph nodes after 15.1 months on study therapy, and progressive mediastinal lymphadenopathy at 19 months. The patient remained alive at time of data cutoff (21 months). During the course of treatment, serum tumor markers were not elevated. All three lesions that were monitored (lung and mediastinum) reduced in size during the course of treatment (Fig. 1b). Both pre- and on-olaparib biopsies were acquired from the left paratracheal mediastinal lymph node. H&E staining showed a major decrease in tumor content (from 90 to 5%) and a marked increase in immune cell infiltration in the on-treatment sample compared to pre-treatment sample (Fig. 2a). The pre-treatment sample was negative for PD-L1 (on-treatment was insufficient for testing). Both pre- and on-treatment samples were negative for hormone receptors (ER, PR) (Fig. 2b). Ki67 was positive in 60–80% of cells pre-treatment and > 50% of cells post-treatment (Table 3). GeneTrails<sup>®</sup> Comprehensive Tumor Panel and WES detected a mutation in *TP53*, amplification of *MYC*, and *RB1* copy loss in the pre-treatment sample (insufficient material was available for on-treatment analysis). The patient had a germline deletion of *BRCA1* exons 13–15 that has been previously linked to familial cancer<sup>25</sup> however, the impact of this deletion on protein function is currently unknown (ClinVar variation ID 89061). The full list of SNVs and CNVs from WES can be found in Supplementary Tables 5 and 6, respectively.

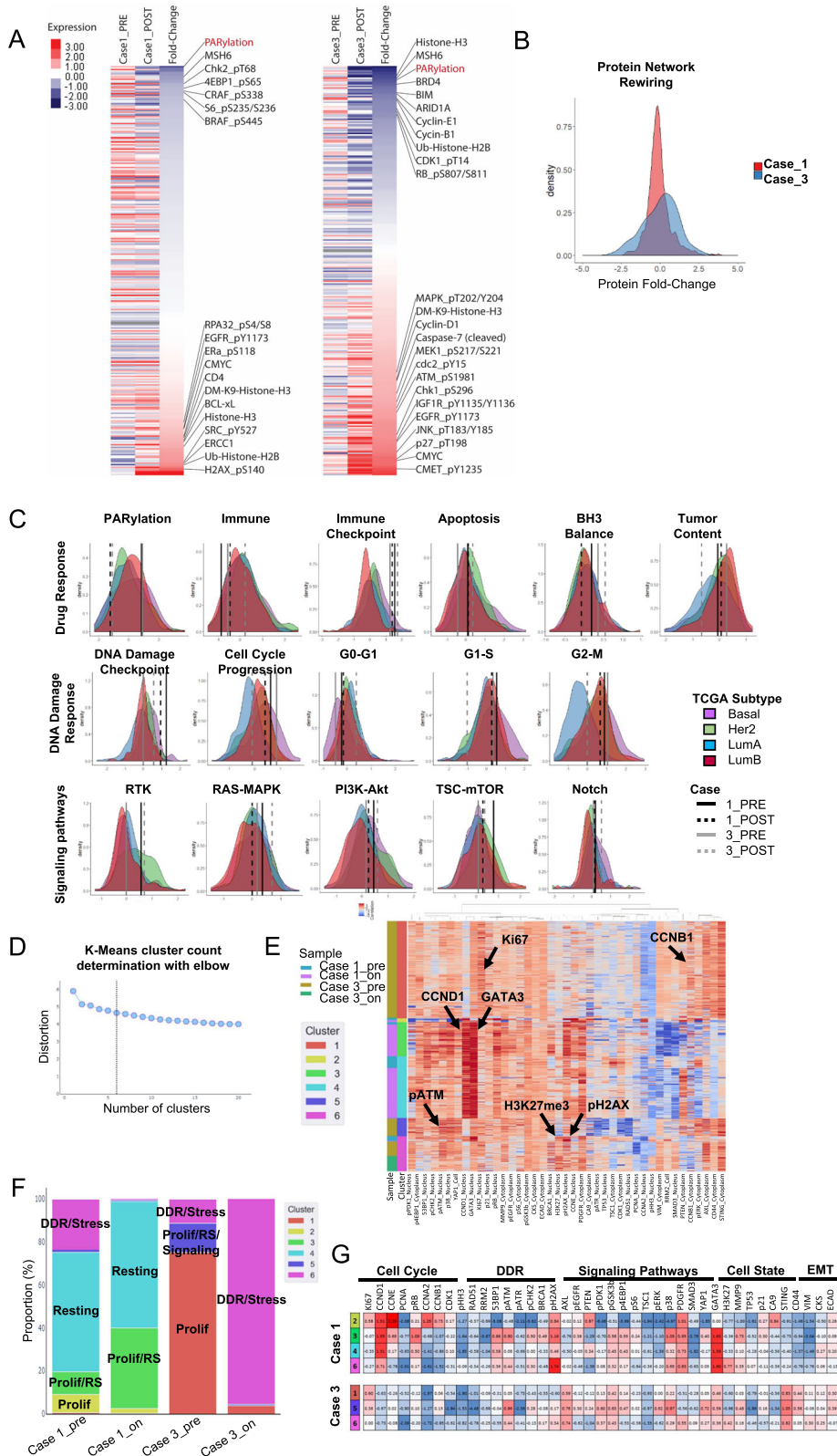
### Immune monitoring during olaparib monotherapy

Several studies including our own have shown that DNA damage induced by PARPi can trigger an immune response and enhance ICB therapy efficacy<sup>7–9,26</sup>. To determine the impact of olaparib treatment on immune cell populations in tumors, pre- and on-treatment samples from patients 1 and 3, and the on-treatment sample from patient 2, were analyzed by mIHC (insufficient material was available from the pre-treatment sample from patient 2). mIHC allows identification and quantification of different immune cell populations on a single FFPE slide.

Furthermore, by analyzing the density of immune cells on the tissue, it is possible to determine if the tumors are immune inflamed, defined as high immune infiltrates (> 250 immune cells/mm<sup>2</sup>)<sup>27</sup>. In patient 1, as shown in Fig. 2c–e, the majority of the immune cells in both biopsies were CD4 + T cells. Although a modest increase in density of CD8 T-cells was observed on-treatment, most were memory or naïve T-cells, with only a small fraction of the CD8 + cells (16 cells/mm<sup>2</sup>) classified as effector cells. Consistent with the progressive disease in this patient, olaparib treatment did not significantly alter the immune composition, at least at this time point. In the case of patient 2, the immune cell population analysis in the on-treatment sample revealed a diverse array of immune cells, with a predominance of CD4 + T-cells and CD163- myelomonocytic cells. The CD8 + T-cell population was small (12 cells/mm<sup>2</sup>), with few effector cells. In contrast, immune cell population analysis from patient 3 revealed important diversity, with CD4 + T-cells and dendritic cells as the predominant populations. Furthermore, the CD8 T-cell population increased (150 cells/mm<sup>2</sup>), and analysis revealed an increase in both early and late effector cell proportions. These results indicate that PARPi activated an immune response in this patient, which is consistent with the subsequent near complete response to the olaparib and durvalumab drug combination.

### Protein network rewiring and adaptive responses

Emerging studies have demonstrated that adaptive responses due to rewiring of cells that survive PARPi-induced stress PARPi can represent therapeutic opportunities<sup>18,20,21</sup>. RPPA analysis was used to compare the pre- and on-treatment protein extracts from cases 1 and 3 (Fig. 3) (insufficient material was available from case 2). There was a drastic decrease in protein PARylation in the on-treatment samples, indicating PARP inhibition by the drug. In patient 1, a DNA damage response (DDR) was triggered by olaparib, as shown by increased phospho-H2AX, phospho-RPA32, and histone modification (Fig. 3a). Interestingly, the drug did not induce a strong overall protein network rewiring in this patient, as shown by the distribution of the protein fold-change (on-treatment/pre-treatment) (Fig. 3b). Furthermore, pathway analysis revealed few changes in the on-treatment sample compared to the pre-treatment (Fig. 3c). Of note, when compared to the TCGA breast cancer cohort, pathway analysis revealed a particularly strong DNA damage checkpoint activity as well as a high cell cycle progression score in both pre and on-treatment samples, indicative of a rapidly growing tumor with replication stress (RS). This, combined with the lack of an immune effector infiltrate (Fig. 2) may indicate greater sensitivity to PARP combined with DNA damage checkpoint inhibitors than to the PARP and anti-PDL1 combination the patient received<sup>20</sup>. Signaling pathways



were highly activated in the baseline biopsy from this patient (RTK, RAS-MAPK, PI3K-AKT, TSC-mTOR), with a slight decrease in the on-treatment sample. Immune score correlated with the multiplex IHC showed a low immune cell infiltration in both pre and on-treatment samples. Taken together, these results suggest that

while PARPi inhibited its target in patient 1, the tumor remained mostly indifferent to the effects of PARP inhibition. By contrast, RPPA analysis of patient 3 samples revealed major protein network rewiring, which consisted of alteration of major signaling pathways, immune activity, and cell cycle proteins



**Fig. 3 Protein network rewiring and single-cell proteomics analysis of the tumor composition.** RPPA analysis was used to analyze protein changes following olaparib treatment. **a** Heat map representing the protein expression in each sample as well as the fold change between on and pre-treatment samples from individual patients. The protein was ordered from the most downregulated to the most upregulated in the on-treatment samples compared to pre-treatment. **b** Distribution plot showing the fold change of each protein during the course of treatment (on-treatment/pre-treatment). **c** Pathway score analysis showing the score distribution of each TCGA breast cancer subtype and the pathway score of each sample from individual patients. **d** Chart constructed using the elbow method to determine the optimal number of clusters for **e** a K-mean clustering analysis identifying different cancer cell populations. Rows represent individual cells and columns represent individual proteins. The first and second columns identifies each patient samples and cell cluster, respectively. **f** Distribution plot showing the percentage of cells from each K-mean cluster within each sample. **g** Table showing the median expression of each protein within each cluster. The table was colored based on expression intensity, with red being high and blue being low expression values.

(Fig. 3a, b). Pathway analysis revealed increased immune cell infiltration, DNA damage checkpoint activation, apoptosis, and increased RTK and RAS-MAPK signaling pathways. Together these changes suggest that multiple PARPi combination therapies could have also led to patient benefit. In addition, a markedly decreased tumor content and cell cycle progression was observed, consistent with the tumor being responsive to the PARPi (Fig. 3c).

Cyc-IF single cell proteomics analysis was used to study changes in tumor heterogeneity and cell state in response to olaparib treatment (Fig. 3d–g, Supplementary Fig. 1). K-means clustering (Fig. 3d, e) of pre and on-treatment samples from both patient 1 and 3 was performed, using the elbow method to determine optimal cluster number. As shown in the heat map, patient 1 displayed high levels of cyclin-D1 and GATA3, supporting findings from DNA sequencing and IHC staining, which indicated an amplification of the *CCND1* gene and elevated expression of AR, respectively. Indeed, GATA3, which is a known target of the ER, has recently been associated with AR expression in TNBC tumors<sup>28,29</sup>. Each of the 6 identified clusters were enriched for different cancer cell populations: (1–2) proliferative, (3) proliferative with RS, (4) resting, (5) proliferative with RS and high protein signaling activity, and (6) DDR and stress. Figure 3f, g illustrate the frequency of different clusters and median expression of each marker across the clusters.

Following olaparib treatment, patient 1 displayed a slight change in population frequencies, with a decrease in the proliferative (high Ki67 and cyclins) and DDR/stress populations (low Ki67 and high DDR proteins) and an increase in proliferating cells that show signs of RS (high DDR proteins, moderate Ki67, and cyclins). More importantly, the resting population (low Ki67, cyclins and DDR proteins, high epithelial markers) remained unchanged, indicating an indifference of this cell population to olaparib. In patient 3, a major restructuring of cell population frequencies was observed following olaparib treatment. In the pre-treatment sample, about 75% of tumor cells were part of the proliferating cluster (high Ki67, low DDR proteins). The remaining 25% were either part of the proliferative/RS/signaling cluster (moderate DDR and cyclins, high signaling activity, and high MMP9 expression) or the DDR/stress cluster (low Ki67 and cyclins, high DDR, and high H3K27me3). In the on-treatment sample, over 90% of the remaining tumor cells became part of the DDR/stress cluster, indicating a strong response to olaparib.

Taken together, baseline and induced changes in RPPA and Cyc-IF may improve the ability to predict tumor response to olaparib, with protein network and cell population changes indicating sensitivity to the effects of PARP inhibition. Indeed, these assays demonstrated a major tumoral restructuring in patient 3, consistent with the tumor ecosystem being sensitive to the effects of PARP inhibition. Conversely, despite inhibition of PARP, patient 1 displayed little protein alteration, suggesting an indifference of the tumor to the effects of PARP inhibition.

## DISCUSSION

The main objective of this study was to establish the feasibility of longitudinal multi-omics analysis of serial tumor samples in

real-time. Here we demonstrated that: (1) serial tumor and blood samples can be collected with minimal risk and analyzed within a 28-day window with CLIA assays, (2) multi-omics analysis of these samples provides complementary information that can help characterize basal states and adaptive responses of the tumor ecosystem to olaparib, (3) changes in tumor state and immune composition following olaparib treatment can be detected within one olaparib cycle and may predict benefit from therapy, and (4) changes in the tumor and ecosystem may aid in the identification of PARPi combinations that could result in therapeutic benefit.

Our previous studies demonstrated that PARPi monotherapy triggers adaptive responses early during the course of treatment, which represents therapeutic opportunities and can be analyzed through the collection of serial samples<sup>18</sup>. This motivated sample collection during PARPi treatment, which would potentially enable us to identify early markers of response and resistance to olaparib. Multi-omics analysis of serially collected samples clearly showed changes in the tumor composition and cell states following therapy initiation confirming our previous observations. Interestingly, there was a strong consensus across the data obtained from different assay types and complementary supporting information that helped illustrate the complexity of each mTNBC tumor and response to treatment. The analysis of a common set of samples across orthogonal platforms was particularly important in determining the consensus across multi-platform assays as well as the robustness and sensitivity of each assay. In terms of detecting genomic aberrations, Genetrails and WES were complementary, with the Genetrails targeted approach being more sensitive but limited by the gene panel that is measured, whereas WES is less sensitive but covers the whole exome. For example, while *CCND1* and *FGF3* gene amplification was detected by both methods in case 1 samples, the *FGFR4* mutation was only detected by Genetrails. Conversely, WES detected several mutations and CNV that were not part of the Genetrails panel and could contain relevant information related to tumor biology. Also, we correlated several of the mutations and copy number alterations with the protein expression data. For example, amplification of *CCND1* and *FGF3*, as well as mutation in *FGFR4* in samples from case 1 correlated with increased *CCND1* protein expression and RTK pathway activity measured by RPPA. Another example of correlation across platforms is given by the high level of AR expression detected by CLIA IHC in both tumor samples from case 1, while ER expression remained low. In these tumors, RPPA as well as Cyc-IF analysis demonstrated that the hormone signaling pathway was activated, supporting the AR as a contributor to tumor biology in this patient. Furthermore, immune cell infiltration observed by H&E in the on-treatment biopsy from patient 3 was consistent across RPPA and mIHC analysis providing greater confidence in the data. The mIHC assay added an important layer of information by describing the different immune cell populations and also allowing analysis of the expression of multiple proteins by a single cell providing a snapshot of immune contexture. Finally, RPPA and Cyc-IF proteomic assays were also shown to be complementary. RPPA “bulk” protein analysis helped identify important pathway alterations in each patient sample, while Cyc-IF helped determine the proportion of cancer cells that

displayed these features. For example, the DNA damage checkpoint measured by RPPA pathway score was activated in both samples from patient 1, suggesting the presence of replication stress. Cyc-IF confirmed two different cancer cell populations with DNA damage response activity in the pre-treatment sample. One of those populations, which occupied a smaller proportion of the tumor was absent from the second biopsy, suggesting these cells were sensitive to therapy. This data integration will be particularly important in the next phase of our study to develop new CLIA assays to predict response to therapy. It will also be interesting to compare the biomarkers that will emerge from this larger trial to the data obtained in other trials that investigated PARPi-based combination therapies. For example, the ISPY2 neoadjuvant trial used a non-trapping PARP inhibitor veliparib in combination with carboplatin or standard chemotherapy and developed a BRAC1ness signature associated to response and the 70-genes signature associated to high risk patients<sup>30,31</sup>.

Although mTNBC is a heterogeneous group of diseases with various molecular aberrations, it is usually treated as a single group, likely contributing to the limited efficacy observed across multiple trials<sup>32</sup>. Indeed, in this study, the patient in case 1 who had rapid progression was AR positive and likely represented a luminal androgen receptor (LAR) subtype of breast cancer. AR expression in breast cancer has been shown to limit effects of PARPi in preclinical models and may explain the indifference of the tumor in case 1 to PARP inhibition<sup>33–35</sup>. Both the MEDIOLA and TOPACIO trials demonstrated activity of PARP and ICB in TNBC. The limited activity particularly in BRCA1/2 wild type tumors may have been influenced by the make-up of the TNBC populations studied. Whether the benefit was limited to patients with basal breast cancer lacking AR expression was not determined in these studies.

PARPi and ICB monotherapies have shown encouraging results in various cancers, but their efficacy is limited in mTNBC patients because of the rapid development of resistance. Previous studies have shown that PARP inhibitors have immunomodulatory properties that have been proposed to increase tumor antigens, antigen presentation, and cytotoxic T-lymphocyte recruitment<sup>26,36</sup>, and upregulate PD-L1 expression through induction of stimulator interferon genes (STING) response and interferon production<sup>6–9</sup>, all of which may increase the efficacy of ICB therapy and extend PARPi efficacy beyond tumors with intrinsic homologous recombination DNA repair deficiency (HRD). In this study, it is likely that tumors from cases 1 and 2 were HR competent, due to the absence of alteration in a set of over 30 genes associated with HR. The tumor from case 3 was most likely HRD, as indicated by the BRCA1 gene alteration and marked response to PARPi monotherapy. This suggested that durvalumab might have added a clinical benefit for case 2. Whether durvalumab contributed to the prolonged response in case 3 cannot be established due to the patient receiving combination therapy, but is likely, given the pronounced immune infiltration detected in the on-therapy sample.

In this pilot study, one of the three patients treated with the drug combination had a stable disease for more than six months and another patient had a near complete response that was sustained for almost two years, indicating that a subset of mTNBC patients and more specifically basal breast cancers with both wild type and mutant BRCA genes could benefit from this drug combination. There is an urgent need to better identify patients that are most likely to benefit from this drug combination. Further, for those patients who are not predicted to benefit from the PARPi and ICB combination, alternative therapy approaches are needed. For those patients whose tumors are unresponsive to inhibition of PARP, it may be optimal to move from PARPi to an alternative drug or drug combination. For those patients for whom there are marked effects of PARPi but no justification for ICB, it may be

optimal to add other drugs to the PARPi, such as AKT or MAPK pathway inhibitors, or DNA damage checkpoint inhibitors, based on changes in the tumor microenvironment. Indeed, we have demonstrated benefit of these combinations in a number of model systems as well as in subpopulations of patients<sup>20–23</sup>. Combination therapies have shown benefit in subpopulations of patients and various models, supporting the concept that identifying biomarkers to direct patients to the appropriate drug combinations could greatly improve patients' outcome. In this study, for example, patient 1 demonstrated no benefit from the olaparib and durvalumab combination; however, benefit might have been seen from the combination of PARPi and DNA damage checkpoint inhibition, based on marked replication stress and DDR activation<sup>20</sup>.

Inherent resistance, characterized by a pre-existing resistance to therapy, is difficult to predict in static biopsies that are acquired prior to therapy. We and other groups have demonstrated in multiple studies that the acquisition of a second biopsy early during the course of treatment is a powerful tool for analyzing how the tumor responds to therapy and for helping to identify mechanisms of adaptive resistance<sup>37</sup>. We have shown that serial samples can be collected pre and on-therapy with minimum risk to the patient and that these samples can be analyzed in "real time" using CLIA assays. Further, we have demonstrated that the serial analysis of tumors under olaparib stress provides information content that is not available from pre-treatment biopsies. The increase in information content available from serial biopsies parallels our results from a window of opportunity trial in ovarian cancer<sup>18</sup>. Indeed, the pathways activated by PARPi in breast cancer cells, as well as the potential combinations indicated by the serial analysis, are remarkably similar in both diseases. The similarity in responses between this study, in which samples were collected at one month, and the ovarian window of opportunity trial, in which samples were collected 10–14 days after initiation of PARP therapy, indicates that biopsies taken earlier in the course of PARP therapy could be informative and allow initiation of rational combination PARPi therapies earlier in patient management. Interestingly, our preliminary data obtained during this pilot study demonstrated a major network restructuring of the tumor for patient 3, who achieved a partial response on therapy, in contrast to the tumor for patient 1, who had progressive disease. This tumor restructuring was observed in multiple assay types (mIHC, RPPA, and Cyc-IF) and did not rely on specific biomarkers, suggesting that changes in tumor states might represent a biomarker of response and further justifies the use of serially collected samples. Although these assays appear to help predict patient response to therapy and could help with clinical decision-making, it will be important to confirm our findings in the larger phase-2 efficacy trials that we are currently conducting.

Based on this pilot study, one of the main challenges that might be encountered during this novel approach is the availability, accessibility, and quality of tissue samples. Unfortunately, as demonstrated by the lack of sufficient tissue from patient 2 to run all planned assays, the quality and amount of tissue available from each biopsy can pose an analytical challenge. Patient 2 had stable disease that could not be clearly characterized through our assays because one of the biopsies did not yield sufficient material to perform RPPA and Cyc-IF. A pre-treatment sample was also not available for immune monitoring through mIHC. Another limitation from collecting biopsies from metastatic lesions is the site of biopsy. There is currently little data that help inform on how the adaptive response to therapy differ from one metastatic site to another. It will be important to further study how therapy alters the microenvironment in different metastatic sites and how cancer cells adaptive responses might be influenced by the tumor microenvironment. The development of additional assays that do not rely on tumor biopsies may increase the probability of being able to identify a patient's response to therapy and rationally



choose a targeted drug combination. The use of serially collected blood samples could represent an opportunity to characterize ctDNA, circulating tumor cells, vesicles, and proteins, and help determine response to therapy. Several studies have shown that serial liquid biopsies can be useful in determining patient response to therapy and can also help identify mechanisms of acquired drug resistance. However, little is understood about the ability to utilize this approach to identify specific adaptive resistance mechanisms of tumor to therapeutic pressure, which would be essential to more successfully identifying potential targeted drug combinations. For these reasons, further studies are needed to confirm if tumor restructuring can be observed from liquid biopsies and if this information can help predict combination therapies.

In conclusion, preclinical models have identified a number of potential PARPi combinations, some of which have been evaluated in early phase clinical trials<sup>6,9,15,18,20–23,33,34,38–44</sup>. However, responses, while encouraging in a subset of patients, remain limited in depth and duration. Additionally, a major limitation of prior trials is relying on archival or pre-treatment tissue, which limits the evaluation of dynamic tumor and tumor ecosystem changes in response to therapy. This pilot study demonstrates the feasibility and the importance of using serial samples to analyze tumor response to olaparib monotherapy in real-time to inform on biomarkers to select patient specific olaparib combination therapies. Deep analysis of serial biopsy samples identified biomarkers that could be used to select patient specific combinations of PARPi with ICB, PARPi and AR in LAR patients, PARPi and DNA damage checkpoint inhibitors targeting ATR, CHK1 or WEE1, or PARPi and inhibitors targeting RTK, PI3K-AKT and RAS-MAPK signaling pathways. These observations need to be confirmed in a larger precision oncology prospective trial such as that we have initiated at the Knight Cancer Institute to refine the utility of dynamic biomarkers of response for particular PARPi combinations. Furthermore, the deep analysis of longitudinal biopsies is expected to identify new mechanisms of response and resistance to therapy as well as novel PARPi combinations that can be explored in future trials.

## METHODS

### Study design and participants

This was a single-center, open-label, single-arm, pilot study of the PARPi olaparib and the PD-L1 antibody durvalumab (Fig. 1a). Eligibility criteria included biopsy proven mTNBC, ECOG PS  $\leq 2$ , received  $\leq 2$  chemotherapeutic courses in the metastatic setting. Patients with prior PARPi or ICB exposure in the metastatic setting were excluded. The study schema is summarized in Fig. 1a. The study was reviewed and approved by the OHSU Institutional Review Board. All participants provided written informed consent to take part in the study.

### Study objectives

The primary objective was to assess the feasibility of completing a suite of Clinical Laboratory Improvement Amendments (CLIA) assays (IHC, Genetrail© Comprehensive Tumor Panel and serum biomarkers) on pre-treatment biopsies within a planned 4-week window for enrolled participants. Secondary objectives included safety and tolerability of the combination; as well as preliminary efficacy endpoints (response rate per RECIST v1.1 and irRECIST, time to disease progression, and overall survival) of olaparib and durvalumab. Exploratory objectives included examining response rates depending on tumor characteristics, identifying candidate predictive biomarkers of sensitivity, identifying emerging candidate mechanisms of resistance to therapy, determining changes in tumor cells induced by PARPi, and identifying any candidate tumor markers that may suggest candidate combinatorial therapies for overcoming treatment resistance.

### Tumor biopsies

Biopsies were performed under ultrasound or CT-guidance using 18 gauge needles. Between 3 and 6 passes were performed on a selected lesion and immediately handed off for: (a) fixation in 10% neutral-buffered formalin; (b) flash-freezing in liquid nitrogen; and (c) fixation in glutaraldehyde. Formalin fixation was for 24 h, after which cores were transferred to 70% ethanol and submitted for routine processing, paraffin embedding and sectioning in a CLIA histology laboratory.

### Immunohistochemistry (IHC)

Five micron sections of tumor biopsies were subjected to immunohistochemistry using Ventana reagents and a Ventana autostainer in a CLIA histology laboratory. Each biopsy, dependent upon sufficient sample, was assessed for the expression of ER, PR, AR, HER2 and Ki67. All stained sections, including H&Es, were scanned on a Leica AT2 digital scanner. PD-L1 IHC 22C3 pharmDx assay was used to qualitatively determine percentage of PD-L1 expression on cancer cells.

### Serum tumor markers

CA15-5, CA27-29 and CEA were measured using standard methodologies in a CLIA laboratory.

### GeneTrails© comprehensive solid tumor panel

This next-generation sequencing panel was run in the Knight Diagnostic Laboratories (CLIA-licensed/CAP-accredited). Tumor-rich areas of unstained five micron sections of FFPE biopsies were macro-dissected and nucleic acid was extracted using a commercial kit. Two separate amplicon-based libraries (one DNA, one RNA/cDNA) were sequenced and analyzed as detailed in Supplementary Method. The DNA library covered 124 cancer-related genes and is used to detect single nucleotide variants, insertions/deletions, copy number alterations, and microsatellite instability.

### Whole exome DNA sequencing and somatic variant calling

To complement Genetrail targeted DNA analysis, whole exome sequencing was used. Total DNA was isolated from FFPE biopsies using QIAGEN FFPE DNA extraction kits. Whole-exome DNA sequencing libraries were prepared from 100–500 ng DNA using KAPA Hyper-Prep Kit (KAPA Biosystems) with Agilent SureSelect XT Target Enrichment System and Human All Exon V5 capture baits (Agilent Technologies). Next generation sequencing was carried out using the Illumina NovaSeq 6000 by Novogene, to produce 150 bp paired end reads with an average depth of 500X tumor/cfDNA or 100X matched normal (buffy coat DNA). FastQ data files were aligned and processed using BWA MEM (0.7.12, GATK, Broad Institute). Somatic variants were called following the GATK Best Practices Somatic Short Variant Discovery, including GATK4 MuTect2 (2.1-beta, Broad Institute). Variants were selected based on the following criteria: tumor  $>30X$ ; normal site depth  $>14X$ ; tumor variant allele frequency  $>5\%$ ; normal vaf  $<2\%$ ; and sites found to be in dbSNP (<https://www.ncbi.nlm.nih.gov/projects/SNP/>) or a panel of normals were removed. All variants were hand-curated with Samtools pileup (1.2, <https://github.com/samtools/samtools>) and Interactive Genome Viewer (2.3.82, Broad Institute) to assess their validity in context. Whole exome tumor copy numbers were estimated using CNVkit (0.9.4a0) of the tumor sample compared to a pool of blood normal samples.

### Multiplex immunohistochemistry, image acquisition and processing

Multiplex IHC was performed on 5  $\mu\text{m}$  FFPE sections using an adapted protocol based on methodology described previously<sup>45,46</sup> and detailed in Supplementary Method. Primary antibody details, dilution, and incubation times are listed in Supplementary Table 1. Cells were classified based on hierarchical gating (image cytometry) and defined as described in Fig. 2. For visualization, signal-extracted images were overlaid in pseudocolor in FIJI.

### Reverse-phase protein array

Protein samples were analyzed by reverse-phase protein array (RPPA) as previously described<sup>47,48</sup>. For scaling purposes, patient data was normalized to TCGA RPPA breast cancer dataset<sup>49</sup>. Heat maps were generated for each patient by ordering proteins from most downregulated to most

upregulated in the on-treatment sample (ratio of treated to pre-treatment). Heat maps were generated using programs Cluster 3.0 and TreeView. Pathway scores for each patient sample (and each sample in the TCGA cohort) were analyzed as previously described<sup>18,49</sup>. A list of protein and phosphoprotein RPPA predictors used to calculate each pathway score is available in Suppl. Table 2.

### Cyclic-immunofluorescence

Cyclic-immunofluorescence (Cyc-IF) allows the detection of more than 40 proteins on a single FFPE slide. Multiple sequential rounds of immunofluorescence staining and quenching were performed on each patient sample as previously described<sup>50–52</sup> and a detailed method can be found in Supplementary Method. Primary antibody details are listed in Suppl. Table 3. The data analysis was performed on python and the codes are available on Github (<https://github.com/biodev/cyclif-workflow/tree/v1.0>).

### Reporting summary

Further information on research design is available in the Nature Research Reporting Summary linked to this article.

### DATA AVAILABILITY

The data generated and analyzed during this study are described in the following data record: <https://doi.org/10.6084/m9.figshare.14186102><sup>53</sup>. The raw DNA sequencing data and the reverse phase protein array data (protein expression data), generated during the current study, are available in the European Genome-Phenome Archive (EGA) repository at the following accession: EGAS00001005479<sup>54</sup>. As these files are controlled access, researchers must request access to the EGA data. The repository also includes clinical and phenotypic metadata and molecular data (including protein expression). HER2 immunohistochemistry data, Intracellular Signaling Protein Panel assay data, and data from the GeneTrails Solid Tumor Panel assay, are not publicly available, but will be made available on reasonable request. Please contact the Knight Diagnostic Laboratories at Oregon Health and Science University (OHSU), email: [KDLClientServices@ohsu.edu](mailto:KDLClientServices@ohsu.edu), for more information on these datasets.

Received: 8 October 2020; Accepted: 22 September 2021;  
Published online: 19 October 2021

### REFERENCES

- Robson, M. et al. Olaparib for metastatic breast cancer in patients with a germline BRCA mutation. *N. Engl. J. Med.* **377**, 523–533 (2017).
- Turner, N. C. et al. A phase II study of talazoparib after platinum or cytotoxic nonplatinum regimens in patients with advanced breast cancer and germline BRCA1/2 mutations (ABRAZO). *Clin. Cancer Res.* **25**, 2717–2724 (2019).
- Robson, M. E. et al. OlympiAD final overall survival and tolerability results: olaparib versus chemotherapy treatment of physician's choice in patients with a germline BRCA mutation and HER2-negative metastatic breast cancer. *Ann. Oncol.* **30**, 558–566 (2019).
- Schmid, P. et al. Atezolizumab and nab-paclitaxel in advanced triple-negative breast cancer. *N. Engl. J. Med.* **379**, 2108–2121 (2018).
- Schmid, P. et al. Atezolizumab plus nab-paclitaxel as first-line treatment for unresectable, locally advanced or metastatic triple-negative breast cancer (IMpassion130): updated efficacy results from a randomised, double-blind, placebo-controlled, phase 3 trial. *Lancet Oncol.* **21**, 44–59 (2020).
- Jiao, S. et al. PARP inhibitor upregulates PD-L1 expression and enhances cancer-associated immunosuppression. *Clin. Cancer Res.* **23**, 3711–3720 (2017).
- Chabanon, R. M. et al. PARP inhibition enhances tumor cell-intrinsic immunity in ERCC1-deficient non-small cell lung cancer. *J. Clin. Investig.* **129**, 1211–1228 (2019).
- Ding, L. et al. PARP inhibition elicits STING-dependent antitumor immunity in Brca1-deficient ovarian cancer. *Cell Rep.* **25**, 2972–2980.e2975 (2018).
- Shen, J. et al. PARPi triggers the STING-dependent immune response and enhances the therapeutic efficacy of immune checkpoint blockade independent of BRCAness. *Cancer Res.* **79**, 311–319 (2019).
- Konstantinopoulos, P. A. in *ESMO*.
- Domchek, S. et al. Phase II study of olaparib (O) and durvalumab (D) (MEDIOLA): updated results in patients (PTS) with germline BRCA-mutated (gBRCAm) metastatic breast cancer (mBC). *Ann. Oncol.* **30**, v475–v532 (2019).
- Domchek, S. M. et al. Abstract PD6-11: an open-label, multitenor, phase II basket study of olaparib and durvalumab (MEDIOLA): Results in germline BRCA-mutated (gBRCAm) HER2-negative metastatic breast cancer (MBC). *Cancer Res.* <https://doi.org/10.1158/1538-7445.SABCS17-PD6-11> (2018).
- Choi, J. I., Park, S. H., Lee, H. J., Lee, D. W. & Lee, H. N. Inhibition of phospho-S6 kinase, a protein involved in the compensatory adaptive response, increases the efficacy of paclitaxel in reducing the viability of matrix-attached ovarian cancer cells. *PLoS ONE* **11**, e0155052 (2016).
- Corcoran, R. B. et al. Combined BRAF, EGFR, and MEK inhibition in patients with BRAF(V600E)-mutant colorectal cancer. *Cancer Discov.* **8**, 428–443 (2018).
- Fang, P. et al. Olaparib-induced adaptive response is disrupted by FOXM1 targeting that enhances sensitivity to PARP inhibition. *Mol. Cancer Res.* **16**, 961–973 (2018).
- Iavarone, C. et al. Combined MEK and BCL-2/XL inhibition is effective in high-grade serous ovarian cancer patient-derived xenograft models and BIM levels are predictive of responsiveness. *Mol. Cancer Ther.* **18**, 642–655 (2019).
- Kurimchak, A. M. et al. Resistance to BET bromodomain inhibitors is mediated by kinase reprogramming in ovarian cancer. *Cell Rep.* **16**, 1273–1286 (2016).
- Labrie, M. et al. Adaptive responses in a PARP inhibitor window of opportunity trial illustrate limited functional interlesional heterogeneity and potential combination therapy options. *Oncotarget* **10**, 3533–3546 (2019).
- Zawistowski, J. S. et al. Enhancer remodeling during adaptive bypass to MEK inhibition is attenuated by pharmacologic targeting of the P-TEFb complex. *Cancer Discov.* **7**, 302–321 (2017).
- Fang, Y. et al. Sequential therapy with PARP and WEE1 inhibitors minimizes toxicity while maintaining efficacy. *Cancer Cell* **35**, 851–867 e857 (2019).
- Sun, C. et al. Rational combination therapy with PARP and MEK inhibitors capitalizes on therapeutic liabilities in RAS mutant cancers. *Sci. Transl. Med.* **9**, <https://doi.org/10.1126/scitranslmed.aal5148> (2017).
- Konstantinopoulos, P. A. et al. Olaparib and alpha-specific PI3K inhibitor alpelisib for patients with epithelial ovarian cancer: a dose-escalation and dose-expansion phase 1b trial. *Lancet Oncol.* **20**, 570–580 (2019).
- Matulonis, U. A. et al. Phase I dose escalation study of the PI3kinase pathway inhibitor BKM120 and the oral poly (ADP ribose) polymerase (PARP) inhibitor olaparib for the treatment of high-grade serous ovarian and breast cancer. *Ann. Oncol.* **28**, 512–518 (2017).
- Mitri, Z. I. et al. Implementing a comprehensive translational oncology platform: from molecular testing to actionability. *J. Transl. Med.* **16**, 358 (2018).
- Seong, M. W. et al. A multi-institutional study of the prevalence of BRCA1 and BRCA2 large genomic rearrangements in familial breast cancer patients. *BMC Cancer* **14**, 645 (2014).
- Huang, J. et al. The PARP1 inhibitor BMN 673 exhibits immunoregulatory effects in a Brca1(-/-) murine model of ovarian cancer. *Biochem. Biophys. Res. Commun.* **463**, 551–556 (2015).
- Keren, L. et al. A structured tumor-immune microenvironment in triple negative breast cancer revealed by multiplexed ion beam imaging. *Cell* **174**, 1373–1387 e1319 (2018).
- Kim, S. et al. Expression patterns of GATA3 and the androgen receptor are strongly correlated in patients with triple-negative breast cancer. *Hum. Pathol.* **55**, 190–195 (2016).
- Naderi, A. & Hughes-Davies, L. A functionally significant cross-talk between androgen receptor and ErbB2 pathways in estrogen receptor negative breast cancer. *Neoplasia* **10**, 542–548 (2008).
- Severson, T. M. et al. The BRCA1ness signature is associated significantly with response to PARP inhibitor treatment versus control in the I-SPY 2 randomized neoadjuvant setting. *Breast Cancer Res.* **19**, 99 (2017).
- Wolf, D. M. et al. DNA repair deficiency biomarkers and the 70-gene ultra-high risk signature as predictors of veliparib/carboplatin response in the I-SPY 2 breast cancer trial. *NPJ Breast Cancer* **3**, 31 (2017).
- Burstein, M. D. et al. Comprehensive genomic analysis identifies novel subtypes and targets of triple-negative breast cancer. *Clin. Cancer Res.* **21**, 1688–1698 (2015).
- Li, L. et al. Androgen receptor inhibitor-induced “BRCAness” and PARP inhibition are synthetically lethal for castration-resistant prostate cancer. *Sci. Signal.* **10**, <https://doi.org/10.1126/scisignal.aam7479> (2017).
- Min, A. et al. Androgen receptor inhibitor enhances the antitumor effect of PARP inhibitor in breast cancer cells by modulating DNA damage response. *Mol. Cancer Ther.* **17**, 2507–2518 (2018).
- Luo, J. et al. The correlation between PARP1 and BRCA1 in AR positive triple-negative breast cancer. *Int. J. Biol. Sci.* **12**, 1500–1510 (2016).
- Galluzzi, L., Senovilla, L., Zitvogel, L. & Kroemer, G. The secret ally: immunostimulation by anticancer drugs. *Nat. Rev. Drug Discov.* **11**, 215–233 (2012).
- Labrie, M. et al. Using reverse phase protein array (RPPA) to identify and target adaptive resistance. *Adv. Exp. Med. Biol.* **1188**, 251–266 (2019).

38. Ibrahim, Y. H. et al. PI3K inhibition impairs BRCA1/2 expression and sensitizes BRCA-proficient triple-negative breast cancer to PARP inhibition. *Cancer Discov.* **2**, 1036–1047 (2012).
39. Juvekar, A. et al. Combining a PI3K inhibitor with a PARP inhibitor provides an effective therapy for BRCA1-related breast cancer. *Cancer Discov.* **2**, 1048–1063 (2012).
40. Liu, J. F. et al. A Phase 1 trial of the poly(ADP-ribose) polymerase inhibitor olaparib (AZD2281) in combination with the anti-angiogenic cediranib (AZD2171) in recurrent epithelial ovarian or triple-negative breast cancer. *Eur. J. Cancer* **49**, 2972–2978 (2013).
41. Sun, C. et al. BRD4 inhibition is synthetic lethal with PARP inhibitors through the induction of homologous recombination deficiency. *Cancer Cell* **33**, 401–416 e408 (2018).
42. Vena, F. et al. MEK inhibition leads to BRCA2 downregulation and sensitization to DNA damaging agents in pancreas and ovarian cancer models. *Oncotarget* **9**, 11592–11603 (2018).
43. Wang, Z. et al. Niraparib activates interferon signaling and potentiates anti-PD-1 antibody efficacy in tumor models. *Sci. Rep.* **9**, 1853 (2019).
44. Yin, Y. et al. Chk1 inhibition potentiates the therapeutic efficacy of PARP inhibitor BMN673 in gastric cancer. *Am. J. Cancer Res* **7**, 473–483 (2017).
45. Tsujikawa, T. et al. Quantitative multiplex immunohistochemistry reveals myeloid-inflamed tumor-immune complexity associated with poor prognosis. *Cell Rep.* **19**, 203–217 (2017).
46. Banik, G. et al. High-dimensional multiplexed immunohistochemical characterization of immune contexture in human cancers. *Methods Enzymol.* **635**, 1–20 (2020).
47. Tibes, R. et al. Reverse phase protein array: validation of a novel proteomic technology and utility for analysis of primary leukemia specimens and hematopoietic stem cells. *Mol. Cancer Ther.* **5**, 2512–2521 (2006).
48. Zhang, L. et al. Serial dilution curve: a new method for analysis of reverse phase protein array data. *Bioinformatics* **25**, 650–654 (2009).
49. Akbani, R. et al. A pan-cancer proteomic perspective on The Cancer Genome Atlas. *Nat. Commun.* **5**, 3887 (2014).
50. Lin, J. R., Fallahi-Sichani, M., Chen, J. Y. & Sorger, P. K. Cyclic immunofluorescence (CyclIF), a highly multiplexed method for single-cell imaging. *Curr. Protoc. Chem. Biol.* **8**, 251–264 (2016).
51. Lin, J. R., Fallahi-Sichani, M. & Sorger, P. K. Highly multiplexed imaging of single cells using a high-throughput cyclic immunofluorescence method. *Nat. Commun.* **6**, 8390 (2015).
52. Lin, J. R. et al. Highly multiplexed immunofluorescence imaging of human tissues and tumors using t-CyclIF and conventional optical microscopes. *Elife* **7**, <https://doi.org/10.7554/eLife.31657> (2018).
53. Labrie, M. et al. Metadata record for the manuscript: Multi-omics analysis of serial samples from metastatic TNBC patients on PARP inhibitor monotherapy provide insight into rational therapy combinations. *figshare* <https://doi.org/10.6084/m9.figshare.14186102> (2021).
54. European Nucleotide Archive <https://identifiers.org/ena.embl:EGAS00001005479> (2021).

## ACKNOWLEDGEMENTS

We gratefully acknowledge the participation, support, and contribution of the SMMART patient advocates Dottie Waddell and Marilyn McWilliams. We also thank the Prospect Creek Foundation and members of the Knight Diagnostic Laboratories (Tanaya Neff, Carol Beadling, Jen Robbins), Knight Biolibrary (Danielle Galipeau) and the Histopathology Shared Resource (Todd Camp). This project was supported by the OHSU Knight Cancer Institute NCI Cancer Center Support Grant P30CA069533. G.B.M.: NCI grant U01CA217842, Komen SAC110052 and Breast Cancer Research Foundation BCRF-19-110. M.L.: Ovarian Cancer Research Alliance and Ruth and Steve Anderson, in honor of Shae Anderson Gerlinger. Y.H.C.: NCI grant U54CA209988 and U2CCA233280. R.B.: DOD PC190174 and PC141395, Veterans Administration Merit Award IBX002842A, NIH R01GM086688 and P30 CA69533, Prospect Creek Foundation. J.W.G.: NIH/NCI U2C CA233280; NIH/NCI U54 CA209988; NIH U54 HG008100; NIH/NCI P30 CA69533; Brenden Colson; PDX Pharmaceuticals, LLC/NCI SRA-14-040 (R44, N43-CO-2013-00078); NIH U01 CA195469, Harvard University Subaward; Susan G. Komen Foundation SAC110012. A.R.G.: R01 DK117459-01, 1 U2C-CA23380-01, The V Foundation for Cancer Research T2015-004. J.G.: U24-CA231877, U2C-CA233280. A.C.: U2C-CA233280. P.T.S.: NIH U24CA210957, U01CA195469, P30CA069533, U01CA199315, U01CA232819, R01CA248383, R01, U01, DOD BC151431P1, Knight Cancer Institute.

## AUTHOR CONTRIBUTIONS

M.L., Z.I.M., G.B.M., A.L. and J.W.G.: article conception and writing. M.L., A.C., C.B., S.S., C.B. and H.M.: experimental design, data acquisition and data analysis. B.J.: biopsy and

sample tissue distribution. A.L., J.K., A.B., Y.H.C., K.C., K.S., S.P., P.T.S., J.G. and L.M.C.: Omics and clinical expertise. Z.I.M., J.V., A.R., M.D., J.Y.L. and L.G.: medical team. A.K.: SMMART Assistant Director, supervision, revision of manuscript. C.L.C.: director of Knight Diagnostic Laboratories, development and analysis of all clinical assays. R.B., J. W.G., Z.I.M. and G.B.M.: Supervision. Z.I.M. and R.B.: Clinical trial support. All authors have been involved in the manuscript revision.

## COMPETING INTERESTS

G.B.M.: Consultant/Scientific Advisory Board (AstraZeneca, Chrysalis, ImmunoMET, Ionis, Lilly USA, LLC, PDX Pharma, SignalChem Lifesciences, Symphogen, Tarveda); Stock/Options/Financial Companies (Catena Pharmaceuticals, ImmunoMet, SignalChem, Spindletop Ventures, Tarveda); Licensed Technology Companies (HRD assay to Myriad Genetics, DSP to Nanostring). C.L.C.: Consultant/Scientific Advisory Board (Amgen, Cepheid/Daneher); Stock/Options (Guardant Health). R.B.: inventor on patents related to KBU2046 and therapeutically targeting cancer motility, and co-owner of Third Coast Therapeutics, which has an option to license those patents; **JV**: Consultant/Scientific Advisory Board (Seattle Genetics/Astellas), research funding (Celldex, Innocin Pharma, Roche/Genentech, Novartis, Merck, Fortis Therapeutics). L. M.C.: paid consultant for Cell Signaling Technologies, received reagent and/or research support from Plexxikon Inc., Pharmacyclics, Inc., Acerta Pharma, LLC, Deciphera Pharmaceuticals, LLC, Genentech, Inc., Roche Glycart AG, Syndax Pharmaceuticals Inc., and NanoString Technologies, and is a member of the Scientific Advisory Boards of Syndax Pharmaceuticals, Carisma Therapeutics, Zymeworks, Inc, Verseau Therapeutics, Kineta, Inc., and Cytomix Therapeutics, Inc. A.R.G.: Siemens Speaker's Bureau, Consultant for Takeda Pharmaceuticals, Inc., Expert Witness for Rice, Dolan & Kershaw and Witherspoon & Kelley. P.T.S.: IP licensed to Cepheid, equity in convergent genomics, consulting for Foundation Medicine. J.G.W.: Business Relationships (Abbott Diagnostics, Danaher (formerly Cepheid), PDX Pharmaceuticals and Thermo Fisher Scientific (formerly FEI), Zeiss, Micron), Company Ownership Positions (Convergent Genomics, KromaTid, PDX Pharmaceuticals), Full- or Part-time Employment or Service as an Officer, Board Member or Other Position of Leadership (Oregon Health & Science University; Cooperative Japan-United States Radiation Effects Research Foundation), Consulting or Advisory Relationships (APOBEC Cancer Program, University of Minnesota; Comprehensive Cancer Center, University of New Mexico (UNM); MJ Murdock Charitable Trust; New Leaf Ventures; Susan G. Komen® for the Cure, University of Denver Medical Center), Stock Ownership (Abbott Diagnostics, AbbVie, Alphabet, Amgen, Amazon, Apple Corporation, Berkshire Hathaway, Cameco, Chevron, ConocoPhillips, Cisco Systems, Clorox, Colgate-Palmolive, Crown Castle, Devon Energy, Disney, Exxon Mobile, General Electric, Gilead, Intel, Nasdaq, Nvidia, PepsiCo, Philips, Procter & Gamble, Swiss Helveita, Walt Disney, Wells Fargo, and Zimmer Biomet). The remaining authors declare no competing interests.

## ADDITIONAL INFORMATION

**Supplementary information** The online version contains supplementary material available at <https://doi.org/10.1038/s41698-021-00232-w>.

**Correspondence** and requests for materials should be addressed to Marilyne Labrie or Zahi I. Mitri.

**Reprints and permission information** is available at <http://www.nature.com/reprints>

**Publisher's note** Springer Nature remains neutral with regard to jurisdictional claims in published maps and institutional affiliations.



**Open Access** This article is licensed under a Creative Commons

Attribution 4.0 International License, which permits use, sharing, adaptation, distribution and reproduction in any medium or format, as long as you give appropriate credit to the original author(s) and the source, provide a link to the Creative Commons license, and indicate if changes were made. The images or other third party material in this article are included in the article's Creative Commons license, unless indicated otherwise in a credit line to the material. If material is not included in the article's Creative Commons license and your intended use is not permitted by statutory regulation or exceeds the permitted use, you will need to obtain permission directly from the copyright holder. To view a copy of this license, visit <http://creativecommons.org/licenses/by/4.0/>.

© The Author(s) 2021